Quantum Electronics **30** (5) 377 – 386 (2000)

INVITED PAPER

PACS numbers: 42.65.Ky
DOI: 10.1070/QE2000v030n05ABEH001728

Complete classification of interaction types for the second-harmonic generation in biaxial nonlinear crystals

S G Grechin, S S Grechin, V G Dmitriev

Abstract. A complete classification of phase-matching directions for the second-harmonic generation in biaxial crystals with quadratic nonlinearity is presented.

1. Introduction

Modern nonlinear optics is characterised by an increase in the number of new nonlinear crystals, on the one hand, and the appearance of new problems, on the other. Among these problems are the frequency conversion of femtosecond laser pulses, frequency tuning of laser radiation, etc. Data presented in handbooks give information on phase-matching parameters for strictly specified crystal cuts used in typical regimes, but give no insight into the functional potentialities of crystals in the solution of unconventional problems.

The aim of the classification proposed by Hobden for the interaction types in the collinear SHG in biaxial crystals, which was given as early as 1967 [1], was to show a variety of possible angular dependences of phase-matching directions in the crystallo-optical coordinate system and their interrelation upon changes, for example, in the fundamental radiation wavelength and crystal temperature and was of vital importance in the development of nonlinear optics.

A further development of the classification [1] was made in Ref. [2], where phase-matching diagrams for the generation of summation and difference frequencies of laser radiation were presented. The classification table of stereographic projections presented in Ref. [1] is often cited in scientific and engineering publications (e.g., see Refs [3, 4]). However, these references are of a purely academic interest and are not related to the analysis of particular crystals or groups of crystals. In attempting to use this classification for the systematisation of presently known crystals, one runs into problems because the calculation results gave stereographic projections that were absent in the classification scheme presented in Ref. [1].

S G Grechin Research Institute of Radio Electronics and Laser Engineering, Bauman Moscow State Technical University, Vtoraya Baumanskaya ul. 5, 107005 Moscow, Russia; e-mail: gera@mx.bmstu.ru
S S Grechin Physics Department, M V Lomonosov State University, Vorob'evy gory, 119899 Moscow, Russia; e-mail: grechin@rf-hp.npi.msu.su
V G Dmitriev 'Polyus' Research Institute, Federal State Unitary Enterprise, ul. Vvedenskogo 3, 117342 Moscow, Russia; e-mail: vgdmitr@orc.ru

Received 25 November 1999
Kvantovaya Elektronika **30** (5) 377 – 386 (2000)
Translated by A N Kirkin; edited by M N Sapozhnikov

The aim of this paper is to give a complete analysis of all possible types of the interaction for the SHG in quadratically nonlinear media with different relations between refractive indices. It will also be shown that one can generalise the representation of results in a form similar to the diagram presented in Fig. 1 in order to analyse not only the phase-matching diagram, but also the feasibility of achieving interactions that are noncritical with respect to the radiation wavelength and temperature.

2. Classification of interaction types in the generation of optical harmonics

In accordance with the commonly accepted classification of the types of interaction in the generation of laser harmonics in biaxial crystals, two types of interaction are possible: ssf (slow-slow-fast) and sff (slow-fast-fast). Note that the last letter corresponds to the second-harmonic wave. Each stereographic projection in Fig. 1 shows the angular distribution of phase-matching directions for the ssf (solid lines) and sff (dashed lines) interactions. The z axis of a crystal is directed perpendicularly upward, the x axis is directed from the right to the left, and the y axis is perpendicular to the plane of Fig. 1. Hereafter, in all the projections, marks on the arcs specify the directions of the optic axis of a crystal.

Depending on the dispersion of birefringence of a crystal (the difference of the principal values of refractive indices) and its variation with the fundamental wavelength, the angular distribution changes by transforming from one projection

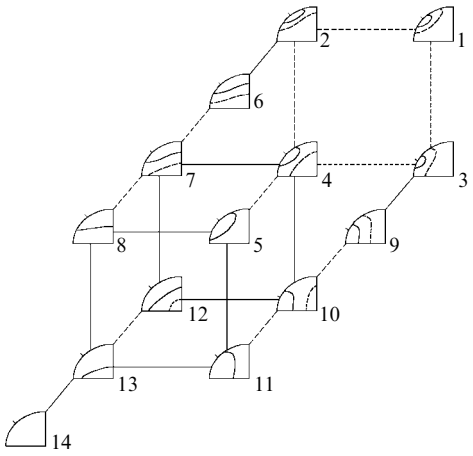

Figure 1. Diagram of stereographic projections of the types of interaction in biaxial crystals.

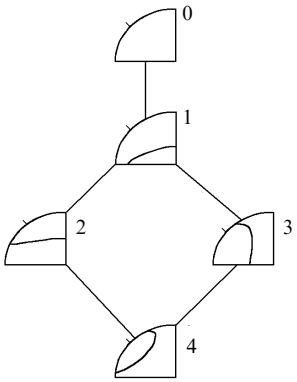

Figure 2. Diagrams for the ssf and sff interactions.

to another in Fig. 1 along the links connecting these projections. This transition is accompanied by a change in the point of intersection of the phase-matching curve with the principal crystal planes (xy, xz, or yz). This point corresponds to the noncritical (with respect to the angle) phase-matching.

Fig. 1 shows the combination of two independent diagrams for each type of interaction. Both diagrams have the same configuration (Fig. 2) corresponding to the appearance of phase matching along the y axis (the change from projection 0 to projection 1 in Fig. 2), for example, with decreasing fundamental wavelength. For projection 1 in Fig. 2, the phase matching noncritical with respect to the angle is realised for certain angles φ (for $\theta = 90^\circ$) and θ (for $\varphi = 90^\circ$) in the planes xy and yz, respectively (φ and θ are the current angular coordinates of the phase-matching directions in the polar coordinate system).

One can see from Fig. 2 that the distribution can change in two different ways depending on the rate of change in the difference of refractive indices: (1) the appearance of phase matching along the x axis and the subsequent appearance of noncritical phase matching in the plane xz (projection 2 in Fig. 2); and (2) a similar process with the appearance of phase matching along the z axis (projection 3) and the subsequent realisation of phase matching in the plane xz. As the wavelength is increased further, we pass in any case (from projections 2 or 3) to projection 4.

As will be shown below, the results presented above (Figs 1 and 2) are totally valid for the ssf interaction. As for the sff interaction, they represent a partial case of a more general case. We will also analyse changes in the angular distributions of phase-matching diagrams for both types of interaction.

2.1 The ssf phase matching

As in Ref. [1] we will consider biaxial crystals in the region of normal dispersion ($n_{2\omega i} > n_{\omega i}$, $i = x, y, z$). According to Ref. [5], the principal values of their refractive indices $n_i(\omega)$ satisfy the relation $n_z(\omega) > n_y(\omega) > n_x(\omega)$ in the entire transparency region. Hereafter, $n_i(\omega)$ is the dependence of the principal values of refractive indices on the radiation frequency, and $n_{\omega i}$ and $n_{2\omega i}$ are the refractive indices at the fundamental frequency and the second-harmonic frequency, respectively.

In contrast to Ref. [1], we will not impose limits on the difference between the principal values of refractive indices:

$$n_{2\omega z} - n_{\omega z} \approx n_{2\omega y} - n_{\omega y} \approx n_{2\omega x} - n_{\omega x} \ll n_{\omega x} \ . \tag{1}$$

All possible configurations of the phase-matching diagrams can be conveniently analysed by using the transitions (links) between stereographic projections for which phase matching is realised along one of the optic axes of a crystal. For certain relations between the refractive indices at both wavelengths, the ssf interaction can be realised along all three crystal axes (x, y, or z). In all these cases, the phase-matching condition $n^{\mathrm{f}}_{2\omega} = n^{\mathrm{s}}_{\omega}$ (where $n^{\mathrm{f}}_{2\omega}$ and n^{s}_{ω} are the refractive indices for the fast and slow waves) has the form

$$n_{2\omega y} = n_{\omega z} \tag{2}$$

along the x axis,

$$n_{2\omega x} = n_{\omega z} \tag{3}$$

along the y axis, and

$$n_{2\omega x} = n_{\omega y} \tag{4}$$

along the z axis.

In the general case, the phase-matching curves intersect the principal planes of a crystal. This takes place for the following relations between refractive indices:

$$n_{2\omega y} > n_{\omega z} > n_{2\omega x} \tag{5}$$

in the plane xy,

$$n_{\omega z} > n_{2\omega x} > n_{\omega y} \tag{6}$$

in the plane yz, and

$$n_{\omega y} > n_{2\omega x} \quad \text{for} \quad \theta < \Omega \ , \tag{7}$$

$$n_{\omega z} > n_{2\omega y} \quad \text{for} \quad \theta > \Omega \tag{8}$$

in the plane xz, where Ω is the angle between the optic axis and the z direction.

The relations between refractive indices providing the realisation of one or other phase-matching diagram (projections in Fig. 2) are determined by the set of conditions (5)–(8), and changes from one projection to another occur when an appropriate combination of conditions (2)–(4) and (5)–(8) occurs.

Fig. 3 presents the dispersion dependences for all possible relations between refractive indices for the type ssf phase matching and the corresponding phase-matching diagrams. The horizontal dashed lines correspond to three refractive indices at the fundamental frequency of laser radiation. On the left of the curves, we give the notation of the principal optic axis of a crystal along which the phase-matching condition is fulfilled. In the region of high radiation frequencies, we have

$$n_{2\omega z} > n_{2\omega y} > n_{2\omega x} > n_{\omega z} > n_{\omega y} > n_{\omega x} \quad \text{or} \quad n_{2\omega x} > n_{\omega z} \ , \tag{9}$$

and the phase-matching conditions are not realised (Fig. 3a). As the radiation wavelength is increased, the tilt angle of all the dispersion dependences decreases, and condition (3) is satisfied at a certain wavelength. This condition corresponds to the appearance of phase matching along the y axis (Fig. 3b). The appearance of phase matching along the y axis is the only version for the ssf interaction because it is commonly assumed that the condition $n_z(\omega) > n_y(\omega) > n_x(\omega)$ is fulfilled in the entire transparency region of a crystal. As the radiation frequency (the tilt angle of the dispersion curve) decreases further, relations (5) and (6) are fulfilled. This corresponds to projection 1 in Fig. 2 (the intersection of the phase-matching curve with the planes xy and yz).

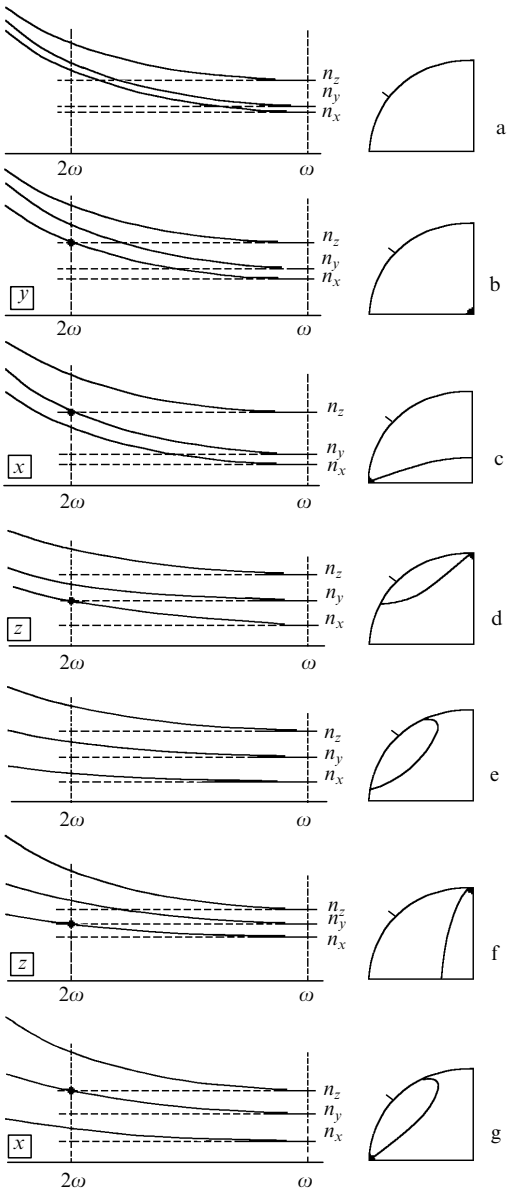

Figure 3. Dispersion dependences of refractive indices for ssf phase matching.

Further on, two versions of the changes in relations between refractive indices are possible. In the first case (the transition along the projections 1 – 2 – 4 in Fig. 2), relation (2) is first satisfied, which corresponds to the phase matching along the x axis (Fig. 3c). Then, variation in the radiation frequency causes a change in projection 2 in Fig. 2, i.e., the intersection of the phase-matching curve with the plane xz (with the angle θ relative to the z axis being greater than the angle Ω). The phase-matching direction may reach the optic axis only in the case of zero dispersion. For projection 2 in Fig. 2, relations (6) and (8) exist. As the refractive indices are changed further, the phase-matching direction in the principal planes of a crystal changes from the plane yz to the plane xz (projection 4 in Fig. 2), which provides phase matching along the z axis (Fig. 3d). In this case, conditions (4) and (8) are fulfilled. Projection 4 in Fig. 2 satisfies relations (7) and (8) (see Fig. 3e).

In the second case (the transition along the projections 1 – 3 – 4 in Fig. 2), the condition for a change in the phase-matching direction from plane yz into plane xz (with $\theta < \Omega$) is first satisfied. When the phase matching along the z axis is realised, relation (4) in combination with (5) is satisfied (Fig. 3f). A further change in the radiation frequency results in a change in projection 3 in Fig. 2., i.e., the intersection of the phase-matching curve with the plane xz. In this case, conditions (5) and (7) are realised. Then, the transition across the crystal axis x [conditions (2) and (7), Fig. 3g] and a further change in projection 4 in Fig. 2 take place.

Table 1.

Projection	Phase-matching planes	Phase-matching conditions
0	–	$n_{2\omega x} > n_{\omega z}$
1	$xy,\ yz$	$n_{2\omega y} > n_{\omega z} > n_{2\omega x} > n_{\omega y}$
2	$xz\ (\theta > \Omega),\ yz$	$n_{\omega z} > n_{2\omega y},\ n_{2\omega x} > n_{\omega y}$
3	$xz\ (\theta < \Omega),\ xy$	$n_{2\omega y} > n_{\omega z},\ n_{\omega y} > n_{2\omega x}$
4	$xz\ (\theta < \Omega),\ xz\ (\theta > \Omega)$	$n_{\omega z} > n_{2\omega y},\ n_{\omega y} > n_{2\omega x}$

Taking into account the general relations determined at the beginning of the paper for the principal values of refractive indices of a crystal in the region of normal dispersion $[n_z(\omega) > n_y(\omega) > n_x(\omega)]$, we present in Table 1 all relations for different projections for the type ssf interaction.

2.2 The sff phase matching

As shown above, for the type ssf interaction, the results presented above agree completely with the results in Ref. [1]. The phase-matching conditions for the type sff interaction, which is determined by the equality $n^{\mathrm{f}}_{2\omega} = (n^{\mathrm{s}}_{\omega} + n^{\mathrm{f}}_{\omega})/2$, change differently. In this case, the phase matching can also be realised along all the principal axes of a crystal:

$$n_{2\omega y} = \tfrac{1}{2}(n_{\omega y} + n_{\omega z}) \tag{10}$$

along the x axis,

$$n_{2\omega x} = \tfrac{1}{2}(n_{\omega x} + n_{\omega z}) \tag{11}$$

along the y axis, and

$$n_{2\omega x} = \tfrac{1}{2}(n_{\omega x} + n_{\omega y}) \tag{12}$$

along the z axis. Relations (10) – (12) can be realised in the general form

$$n_{2\omega k} = \tfrac{1}{2}(n_{\omega k} + n_{\omega j})\ , \tag{13}$$

where $k = x,\ y$ and $j = y,\ z$.

In the region between these limiting states, the phase-matching curve intersects the principal planes of a crystal, which is realised for the following relations between refractive indices:

$$n_{2\omega y} > \tfrac{1}{2}(n_{\omega y} + n_{\omega z})\ , \quad n_{2\omega x} < \tfrac{1}{2}(n_{\omega x} + n_{\omega z}) \tag{14}$$

or

$$n_{2\omega y} < \tfrac{1}{2}(n_{\omega y} + n_{\omega z})\ , \quad n_{2\omega x} > \tfrac{1}{2}(n_{\omega x} + n_{\omega z}) \tag{15}$$

in the plane xy,

$$n_{2\omega x} > \tfrac{1}{2}(n_{\omega x} + n_{\omega y})\ , \quad n_{2\omega x} < \tfrac{1}{2}(n_{\omega x} + n_{\omega z}) \tag{16}$$

in the plane yz, and

$$n_{2\omega x} < \tfrac{1}{2}(n_{\omega x} + n_{\omega y}) \quad \text{for} \quad \theta < \Omega\,, \qquad (17)$$
$$n_{2\omega z} > \tfrac{1}{2}(n_{\omega y} + n_{\omega z}) \quad \text{for} \quad \theta < \Omega\,,$$
$$n_{2\omega y} < \tfrac{1}{2}(n_{\omega y} + n_{\omega z}) \quad \text{for} \quad \theta > \Omega\,, \qquad (18)$$
$$n_{2\omega y} > \tfrac{1}{2}(n_{\omega x} + n_{\omega y}) \quad \text{for} \quad \theta > \Omega\,,$$

in the plane xz.

Here, as in the case of the ssf interaction, phase matching in the planes yz or xy is possible only for a single relation between refractive indices. For phase matching in the plane xy, relations (14) and (15) are valid. This follows from the fact that conditions (16) – (18) are determined by the intersection of a circle and an ellipse for refractive indices at the wavelengths of fundamental radiation and the second harmonic; they are unique because of the general relations determined above for the refractive indices. The existence of phase matching in the plane xy is determined by the intersection of two ellipses. Relations (14) and (15) differ only by the inequality sign. It is evident that each of these pairs of inequalities is compatible. In what follows, we exclude from consideration the second inequalities in relations (17) and (18) because of their identity.

The dispersion dependences of refractive indices $n_i(\omega)$, which characterise possible changes in the phase-matching curve, and the corresponding distributions of phase-matching directions are presented in Fig. 4. The horizontal dashed lines correspond to three half-sums of refractive indices (13). On the left of the curves (as in Fig. 3), we give the notation of the principal axis of a crystal along which the phase-matching condition is fulfilled. The initial case when the phase-matching condition for the sff interaction is absent is characterised by the following relations between the principal values of refractive indices (Fig. 4a):

$$n_{2\omega y} > \tfrac{1}{2}(n_{\omega y} + n_{\omega z})\,, \quad n_{2\omega x} > \tfrac{1}{2}(n_{\omega x} + n_{\omega z})\,. \qquad (19)$$

Note that the equalities $n_{2\omega x} = (n_{\omega x} + n_{\omega z})/2$ and $n_{2\omega y} = (n_{\omega y} + n_{\omega z})/2$ do not represent the phase-matching conditions. Consider various possible versions of changes in phase-matching directions.

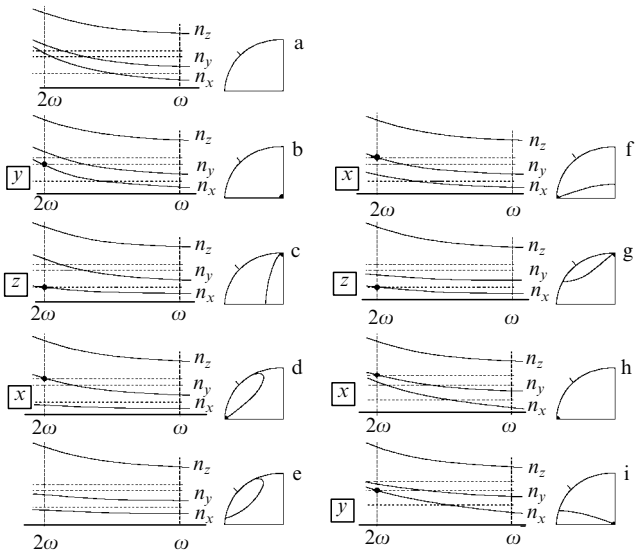

Figure 4. Dispersion dependences of refractive indices for sff phase matching.

The fulfilment of condition (11) corresponds to the appearance of phase matching only along the y axis (Fig. 4b), which is similar to the case discussed above for the ssf interaction (Fig. 3b). The process may go further in two directions. In the first case, changes in phase-matching directions are caused by rapid changes in $n_x(\omega)$ (a strong dispersion). When relation (11) is satisfied, this leads to the appearance of phase matching in the planes xy and yz (projection 1 in Fig. 2), which is characterised by the joint fulfilment of conditions (14) and (16). One can easily see that conditions (15) and (16) are incompatible. As the refractive indices change further, phase matching along the z axis (Fig. 4c) is realised. This corresponds to the joint fulfilment of conditions (12) and (14). A further change in the refractive indices causes a change in projection 3 in Fig. 2. In this case, relations (14) and (17) are not fulfilled, and conditions (15) and (17) are incompatible. Later on, phase matching along the x axis appears [Fig. 4d, conditions (10) and (17)], and subsequently the phase-matching curve intersects the plane xz (above the optic axis and below it) at two points (Fig. 4e). In this case, relations (17) and (18) are fulfilled.

In the second case, after achieving projection 1 in Fig. 2, a strong dispersion $n_y(\omega)$ is observed, and the phase matching along the x axis appears [Fig. 4f, conditions (10) and (16)]. Then, a change in projection 2 in Fig. 2 occurs, and relations (16) and (18) for refractive indices are fulfilled. Subsequently, phase matching along the z axis appears [Fig. 4g, conditions (12) and (18)], and the change to projection 4 in Fig. 2 occurs [conditions (17) and (18)].

In addition to the change from projection 0 to projection 1 in Fig. 2 (the appearance of phase matching along the y axis), an initial appearance of phase matching along the x axis [condition (10)] under conditions of strong dispersion of $n_x(\omega)$ and weak dispersion of $n_y(\omega)$ is also possible (Fig. 4h). After the appearance of phase matching along the x axis, the phase-matching directions intersect the planes xy and xz of a crystal. In this case, conditions (15) and (18) are fulfilled. A further change in the refractive indices leads to the appearance of phase matching along the y axis [Fig. 4i, conditions (16) and (18)], i.e., the change in projection 2 in Fig. 2. Then, the change from one projection to another is similar to the change from projection 2 to projection 4 considered above (Fig. 2).

In contrast to Fig. 2 we have one more phase-matching diagram for the sff interaction. This diagram represents a conic surface with a bisectrix along the x axis (projection 5 in Fig. 5). The system of all projections connected by allowed transitions (links) gives the diagram presented in Fig. 5. It shows three possible versions of a transition: 0 – 1 – 3 – 4, 0 – 5 – 2 – 4, and 0 – 1 – 2 – 4. The letters A and B in Fig. 5 denote the points of intersection of the phase-matching curves with the principal planes of a crystal, which correspond to the interactions that are noncritical with respect to the angles. Point A in projection 4 corresponds to the phase-matching angles $\theta > \Omega$, and point B corresponds to the angles $\theta > \Omega$.

Projections 3 and 5 are identical in form (with respect to the intersection of the principal planes of a crystal by the phase-matching curves), but the positions of points A and B show that the processes of transformation of these projections (a change from the preceding projection to the subsequent one) are different. We have $\theta > \Omega$ for point A

Table 2.

Projection	Phase-matching planes	Phase-matching conditions
0	–	
$n_{2\omega y} > (n_{\omega y} + n_{\omega z})/2,\ n_{2\omega x} > (n_{\omega x} + n_{\omega z})/2$	1	$xy,\ yz$
$n_{2\omega y} > (n_{\omega y} + n_{\omega z})/2,\ (n_{\omega x} + n_{\omega z})/2 > n_{2\omega x} > (n_{\omega x} + n_{\omega y})/2$	2	$xz\ (\theta > \Omega),\ yz$
$(n_{\omega y} + n_{\omega z})/2 > n_{2\omega y},\ (n_{\omega x} + n_{\omega z})/2 > n_{2\omega x} > (n_{\omega x} + n_{\omega y})/2$	3	$xz\ (\theta < \Omega),\ xy$
$n_{2\omega y} > (n_{\omega y} + n_{\omega z})/2,\ (n_{\omega x} + n_{\omega y})/2 > n_{2\omega x}$	4	$xz\ (\theta < \Omega),\ xz\ (\theta > \Omega)$
$(n_{\omega y} + n_{\omega z})/2 > n_{2\omega y},\ (n_{\omega x} + n_{\omega y})/2 > n_{2\omega x}$	5	$xy,\ xz\,(\theta > \Omega)$
$(n_{\omega y} + n_{\omega z})/2 > n_{2\omega y},\ n_{2\omega x} > (n_{\omega x} + n_{\omega z})/2$		

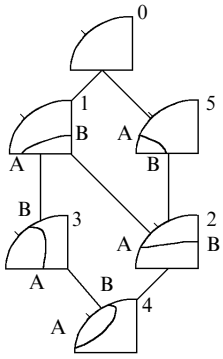

Figure 5. Diagram for the sff interaction.

in projection 5 and $\theta < \Omega$ for point B in projection 3. The direct transition between projections 3 and 5 is impossible because it requires that two crystal axes be simultaneously intersected by the phase-matching curve. The conditions corresponding to all the projections of the sff interaction in Fig. 5, i.e., the relations between refractive indices, are presented in Table 2.

3. Complete configuration diagram

The diagrams in Fig. 2 (for the ssf interaction) and Fig. 5 (for the sff interaction) may be combined into a single diagram similar to the one shown in Fig. 1. The complete diagram of projections is shown in Fig. 6. Here, in contrast to the diagram in Fig. 1, where the continuous numbering of projections was used, we use double numbering. The first number corresponds to the ssf interaction, and the second number corresponds to the sff interaction. This approach allows us to simplify the further analysis of distribution changes. Here, we have two new elements (projections 25 and 45) in comparison with Fig. 1, and they correspond to the appearance of the sff phase matching along the x axis. They are connected with other projections by the corresponding links.

For each of the projections in the diagram in Fig. 6, the relation between refractive indices is determined by the corresponding conditions for the ssf and sff interactions from Tables 1 and 2. One can show directly that projection 5 for the sff interaction (Fig. 5) is compatible only with projections 2 and 4 for the ssf interaction (Fig. 2)

Thus we have two more possible configurations of phase-matching directions [projections 25 and 45 (Fig. 6)] in addition to the configurations presented in Fig. 1. The phase matching along the x axis can appear only for the sff interaction and cannot be realised for the ssf interaction because the phase-matching conditions for all principal planes of a crystal are specified by the intersection of a circle and an

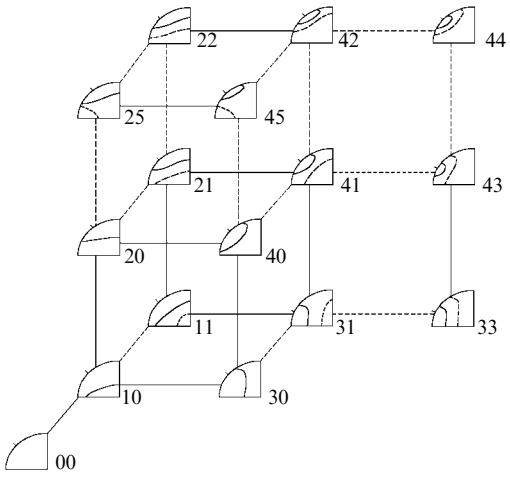

Figure 6. Diagram of stereographic projections of phase-matching directions for all types of interaction upon SHG in biaxial crystals $[n_z(\omega) > n_y(\omega) > n_x(\omega)]$.

ellipse. In Table 3 we present inequalities for the principal values of refractive indices for all the projections in Fig. 6. They were obtained from Tables 1 and 2 by excluding redundant relations.

The distribution corresponding to projection 5 in Fig. 5 can be realised only for the crystals with different dispersions $n_x(\omega)$ and $n_y(\omega)$. After some simple manipulations, we obtain the dispersion relation for the components of refractive indices from expression (15):

$$n_{2\omega x} - n_{\omega x} > n_{2\omega y} - n_{\omega y}\ .$$

This condition is fulfilled, for example, for the crystals having 'isopoints,' i.e., wavelengths for which the difference $n_y(\omega) - n_x(\omega)$ vanishes (a uniaxial crystal) and then its sign changes to the negative one (e.g., see Ref. [6]).

In accordance with the IEEE/ANSI Std. 176 – 1987 convention, the crystallo-optical coordinate system is chosen so that the condition $n_z(\omega) > n_y(\omega) > n_x(\omega)$ can be fulfilled. This is a conventional, so-called optical, arrangement of a crystal. The crystal is said to be positive (negative) if the angle 2Ω between the optic axes is smaller (larger) than 90 °. In practice (e.g., see Ref. [7]), these relations for refractive indices are not fulfilled.

Table 4 presents some parameters of the most extensively used crystals, including the relations between orientations of axes in the crystallo-optical (xyz) and crystallo-physical (abc) coordinate systems. For many crystals, the parameters presented above do not satisfy the recommendations of the convention. Consider a complete phase-matching diagram for the crystals satisfying the relation $n_x(\omega) > n_y(\omega) > n_z(\omega)$.

Table 3.

Projection	Phase-matching conditions	
	sff type	ssf type
40	$n_{2\omega y} > (n_{\omega y} + n_{\omega z})/2,\ n_{2\omega x} > (n_{\omega x} + n_{\omega z})/2$	$n_{\omega z} > n_{2\omega y},\ n_{\omega y} > n_{2\omega x}$
41	$n_{2\omega y} > (n_{\omega y} + n_{\omega z})/2,\ (n_{\omega x} + n_{\omega z})/2 > n_{2\omega x} > (n_{\omega x} + n_{\omega y})/2$	
42	$(n_{\omega y} + n_{\omega z})/2 > n_{2\omega y},\ (n_{\omega x} + n_{\omega z})/2 > n_{2\omega x} > (n_{\omega x} + n_{\omega y})/2$	
43	$n_{2\omega y} > (n_{\omega y} + n_{\omega z})/2,\ (n_{\omega x} + n_{\omega y})/2 > n_{2\omega x}$	
44	$(n_{\omega y} + n_{\omega z})/2 > n_{2\omega y},\ (n_{\omega x} + n_{\omega y})/2 > n_{2\omega x}$	
45	$(n_{\omega y} + n_{\omega z})/2 > n_{2\omega y},\ n_{2\omega x} > (n_{\omega x} + n_{\omega z})/2$	
20	$n_{2\omega y} > (n_{\omega y} + n_{\omega z})/2,\ n_{2\omega x} > (n_{\omega x} + n_{\omega z})/2$	$n_{\omega z} > n_{2\omega y},\ n_{2\omega x} > n_{\omega y}$
21	$n_{2\omega y} > (n_{\omega y} + n_{\omega z})/2,\ (n_{\omega x} + n_{\omega z})/2 > n_{2\omega x}$	
22	$(n_{\omega y} + n_{\omega z})/2 > n_{2\omega y},\ (n_{\omega x} + n_{\omega z})/2 > n_{2\omega x}$	
25	$(n_{\omega y} + n_{\omega z})/2 > n_{2\omega y},\ n_{2\omega x} > (n_{\omega x} + n_{\omega z})/2$	
30	$n_{2\omega x} > (n_{\omega x} + n_{\omega z})/2$	$n_{2\omega y} > n_{\omega z},\ n_{\omega y} > n_{2\omega x}$
31	$(n_{\omega x} + n_{\omega z})/2 > n_{2\omega x} > (n_{\omega x} + n_{\omega y})/2$	
33	$(n_{\omega x} + n_{\omega y})/2 > n_{2\omega x}$	
10	$n_{2\omega x} > (n_{\omega x} + n_{\omega z})/2$	$n_{2\omega y} > n_{\omega z} > n_{2\omega x} > n_{\omega y}$
11	$(n_{\omega x} + n_{\omega z})/2 > n_{2\omega x}$	
00	–	$n_{2\omega x} > n_{\omega z}$

Table 4.

Crystal	Crystal sign	Relation between n_i	$2\Omega\,/^\circ$	λ/nm	xyz
BAMB	–	$n_x > n_y > n_z$	57.25	532.1	*abc*
Banan	–	$n_x > n_y > n_z$	13	–	*abc*
KCN	–	$n_z > n_y > n_x$	115.2	546.1	*bca*
KLN	–	$n_z > n_y > n_x$	111	546.1	*bca*
LBO	–	$n_z > n_y > n_x$	109.2	532.1	*acb*
LFM	–	$n_z > n_y > n_x$	123.8	532.1	*abc*
LGO	–	$n_z > n_y > n_x$	74.5	500	*bca*
MDNB	–	$n_x > n_y > n_z$	51.15	532.1	*abc*
MBF	–	$n_z > n_y > n_x$	117.5	532.1	*bca*
KNB	–	$n_x > n_y > n_z$	66.78	532.1	*bac*
SFM	–	$n_z > n_y > n_x$	92.5	540	*abc*
α-HIO_3	–	$n_x > n_y > n_z$	47	–	*bca*
COANP	+	$n_z > n_y > n_x$	36.13	547	*cab*
KTP	+	$n_z > n_y > n_x$	37.4	546.1	*abc*
KTA	+	$n_z > n_y > n_x$	34.5	532.1	*abc*
CTA	+	$n_z > n_y > n_x$	52.9	532.1	*abc*
RTA	+	$n_z > n_y > n_x$	39.4	–	*abc*
KB5	+	$n_x > n_y > n_z$	126.3	546.1	*abc*
DKB5	+	$n_x > n_y > n_z$	–	–	*abc*
L-CTT	+	$n_z > n_y > n_x$	65.8	532.1	*acb*
MMONS	+	$n_z > n_y > n_x$	70.2	543	*abc*
$NaNO_2$	+	$n_z > n_y > n_x$	62.5	532.5	*acb*

Note: BAMB, bis(aminomethyl)benzene; Banan, barium sodium niobate ($Ba_2NaNb_5O_15$); KCN, potassium-cerium nitrate dihydrate ($K_2Ce(NO_3)_5 \times 2H_2O$); KLN, potassium-lanthanum nitrate dihydrate ($K_2La(NO_3)_5 \times 2H_2O$); LBO, lithium triborate (LiB_3O_5); LFM, lithium formate ($LiCOOH \times H_2O$); LGO, lithium gallate ($LiGaO_2$); MDNB, metadinitrobenzene [$C_6H_4(NO_2)_2$]; MBF, magnesium-barium fluoride ($MgBaF_4$); KNB, potassium niobate ($KNbO_3$); SFM, sodium formate ($NaCOOH$); α-HIO_3, iodic acid; COANP, 2-cycloactylamino-5-nitropyridine; KTP, potassium titanyl phosphate ($KTiOPO_4$); KTA, potassium titanyl arsenate ($KTiOAsO_4$); CTA, caesium titanyl arsenate ($CsTiOAsO_4$); RTA, rubidium titanyl arsenate ($RbTiOAsO_4$); KB5, potassium pentaborate ($KB_5O_8 \times 4H_2O$); DKB5, deuterated potassium pentaborate ($KB_5O_8 \times 4D_2O$); L-CTT, calcium tartrate tetrahydrate ($CaC_4H_4O_6 \times 4H_2O$); MMONS, 3-methyl-4-methox*y*-4′-nitrostilbene.

The phase-matching directions for the ssf interaction lie in the principal planes of a crystal under the following conditions:

$$n_{\omega x} > n_{2\omega z} > n_{\omega y} \tag{20}$$

in the plane xy,

$$n_{2\omega y} > n_{\omega x} > n_{2\omega z} \tag{21}$$

in the plane yz, and

Table 5.

Projection	Phase-matching planes	Phase-matching conditions
0	–	$n_{2\omega z} > n_{\omega x}$
1	$xy,\ yz$	$n_{2\omega y} > n_{\omega x} > n_{2\omega z} > n_{\omega y}$
2	$xz\ (\theta > \Omega),\ yz$	$n_{2\omega y} > n_{\omega x},\ n_{\omega y} > n_{2\omega z}$
3	$xz\ (\theta < \Omega),\ xy$	$n_{\omega x} > n_{2\omega y},\ n_{2\omega z} > n_{\omega y}$
4	$xz\ (\theta < \Omega),\ xz\ (\theta > \Omega)$	$n_{\omega x} > n_{2\omega y},\ n_{\omega y} > n_{2\omega z}$

$$n_{\omega x} > n_{2\omega y} \quad \text{for} \quad \theta < \Omega\,, \tag{22}$$

$$n_{2\omega x} > n_{\omega y} \quad \text{for} \quad \theta > \Omega \tag{23}$$

in the plane xz.

For the ssf interaction, all distributions (projections) and the relation between them, similar to those shown in Fig. 2, are possible. Analogous to Table 2, we present the conditions providing the realisation of all possible projections in Table 5. The sff interaction is distinct in that the phase-matching conditions in the principal planes xz (for $\theta > \Omega$ and $\theta > \Omega$) and xy are determined by the intersection of a circle and an ellipse and therefore have a single condition for realisation, whereas the phase-matching condition in the plane yz is determined by the intersection of two ellipses for refractive indices. In this case, by analogy with conditions (14) and (15) for the sff interaction for $n_z(\omega) > n_y(\omega) > n_x(\omega)$, we have two possible conditions under which phase matching in the plane yz takes place. For all the principal planes, the relations between refractive indices have the form

$$\begin{aligned} &n_{2\omega z} > \tfrac{1}{2}(n_{\omega y} + n_{\omega z})\,, \\ &n_{2\omega z} < \tfrac{1}{2}(n_{\omega x} + n_{\omega z}) \end{aligned} \tag{24}$$

in the plane xy,

$$\begin{aligned} &n_{2\omega y} > \tfrac{1}{2}(n_{\omega x} + n_{\omega y})\,, \\ &n_{2\omega z} < \tfrac{1}{2}(n_{\omega x} + n_{\omega z}) \end{aligned} \tag{25}$$

or

$$\begin{aligned} &n_{2\omega y} < \tfrac{1}{2}(n_{\omega x} + n_{\omega y})\,, \\ &n_{2\omega y} > \tfrac{1}{2}(n_{\omega x} + n_{\omega y}) \end{aligned} \tag{26}$$

in the plane yz, and

$$\begin{aligned} &n_{2\omega y} < \tfrac{1}{2}(n_{\omega x} + n_{\omega y}) \quad \text{for} \quad \theta < \Omega\,, \\ &n_{2\omega y} > \tfrac{1}{2}(n_{\omega y} + n_{\omega z}) \quad \text{for} \quad \theta < \Omega\,, \end{aligned} \tag{27}$$

$$\begin{aligned} &n_{2\omega z} < \tfrac{1}{2}(n_{\omega y} + n_{\omega z}) \quad \text{for} \quad \theta > \Omega\,, \\ &n_{2\omega x} > \tfrac{1}{2}(n_{\omega x} + n_{\omega y}) \quad \text{for} \quad \theta > \Omega \end{aligned} \tag{28}$$

in the plane xz.

From expressions (24) – (28) it follows that in the case under consideration, in contrast to Fig. 5, phase matching can be realised not only along the x axis, but also along the z axis. Table 6 presents the conditions for refractive indices providing the realisation of all possible distributions of phase-matching directions for the sff interaction.

A complete diagram of projections for the sff interaction is presented in Fig. 7. Its main distinction from the diagram in Fig. 5 is that only a single transition to projection 3 is possible upon the appearance of phase matching along the z axis (projection 5 in Fig. 7). Combining diagrams in Figs 2 and 7, one obtains a complete diagram for all combinations of

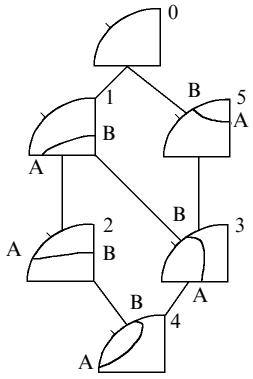

Figure 7. Diagram for the sff interaction.

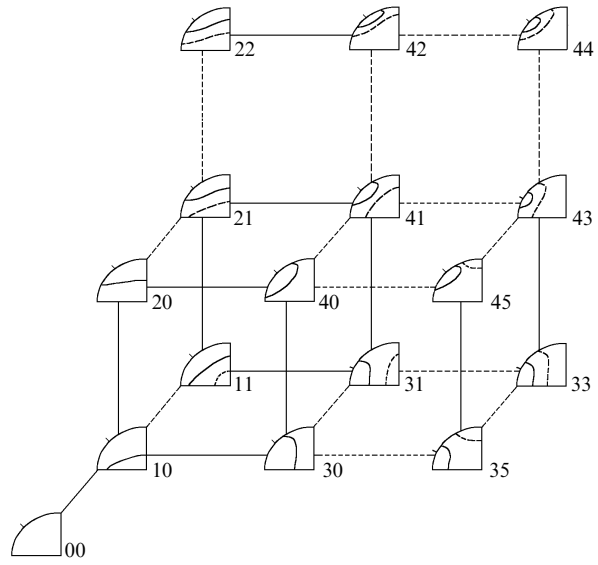

Figure 8. Diagram of stereographic projections of phase-matching directions for all types of interaction upon SHG in biaxial crystals $[n_x(\omega) > n_y(\omega) > n_z(\omega)]$

Table 6.

Projection	Phase-matching planes	Phase-matching conditions
0	–	
$n_{2\omega y} > (n_{\omega x} + n_{\omega y})/2,\ n_{2\omega z} > (n_{\omega x} + n_{\omega z})/2$	1	$xy,\ yz$
$n_{2\omega y} > (n_{\omega x} + n_{\omega y})/2,\ (n_{\omega x} + n_{\omega z})/2 > n_{2\omega z} > (n_{\omega y} + n_{\omega z})/2$	2	$xz\ (\theta > \Omega),\ yz$
$(n_{\omega x} + n_{\omega z})/2 > n_{2\omega z},\ n_{2\omega y} > (n_{\omega x} + n_{\omega y})/2$	3	$xz\ (\theta < \Omega),\ xy$
$n_{2\omega y} < (n_{\omega x} + n_{\omega y})/2,\ (n_{\omega x} + n_{\omega z})/2 > n_{2\omega z} > (n_{\omega x} + n_{\omega y})/2$	4	$xz\ (\theta < \Omega),\ xz\ (\theta > \Omega)$
$(n_{\omega x} + n_{\omega y})/2 > n_{2\omega y},\ (n_{\omega y} + n_{\omega z})/2 > n_{2\omega z}$	5	$yz,\ xz\,(\theta < \Omega)$
$(n_{\omega x} + n_{\omega y})/2 > n_{2\omega y},\ n_{2\omega z} > (n_{\omega x} + n_{\omega z})/2$		

Table 7.

Projection	Phase-matching conditions	
	sff type	ssf type
40	$n_{2\omega y} > (n_{\omega y} + n_{\omega x})/2,\ n_{2\omega z} > (n_{\omega x} + n_{\omega z})/2$	$n_{\omega x} > n_{2\omega y},\ n_{\omega y} > n_{2\omega z}$
41	$n_{2\omega y} > (n_{\omega y} + n_{\omega x})/2,\ (n_{\omega x} + n_{\omega z})/2 > n_{2\omega z} > (n_{\omega z} + n_{\omega y})/2$	
42	$n_{2\omega y} > (n_{\omega y} + n_{\omega x})/2,\ (n_{\omega y} + n_{\omega z})/2 > n_{2\omega z}$	
43	$(n_{\omega x} + n_{\omega z})/2 > n_{2\omega z} > (n_{\omega y} + n_{\omega z})/2,\ (n_{\omega x} + n_{\omega y})/2 > n_{2\omega y}$	
44	$(n_{\omega y} + n_{\omega x})/2 > n_{2\omega y},\ (n_{\omega z} + n_{\omega y})/2 > n_{2\omega z}$	
45	$(n_{\omega y} + n_{\omega x})/2 > n_{2\omega y},\ n_{2\omega z} > (n_{\omega x} + n_{\omega z})/2$	
30	$n_{2\omega y} > (n_{\omega y} + n_{\omega x})/2,\ n_{2\omega z} > (n_{\omega x} + n_{\omega z})/2$	$n_{\omega x} > n_{2\omega y},\ n_{2\omega z} > n_{\omega y}$
31	$n_{2\omega y} > (n_{\omega y} + n_{\omega x})/2,\ (n_{\omega x} + n_{\omega z})/2 > n_{2\omega z}$	
32	$(n_{\omega x} + n_{\omega z})/2 > n_{2\omega z},\ (n_{\omega x} + n_{\omega y})/2 > n_{2\omega y}$	
35	$(n_{\omega y} + n_{\omega x})/2 > n_{2\omega y},\ n_{2\omega z} > (n_{\omega x} + n_{\omega z})/2$	
20	$n_{2\omega z} > (n_{\omega x} + n_{\omega z})/2$	$n_{2\omega y} > n_{\omega x},\ n_{\omega y} > n_{2\omega z}$
21	$(n_{\omega x} + n_{\omega z})/2 > n_{2\omega z} > (n_{\omega z} + n_{\omega y})/2$	
22	$(n_{\omega z} + n_{\omega y})/2 > n_{2\omega z}$	
10	$n_{2\omega z} > (n_{\omega x} + n_{\omega z})/2$	$n_{2\omega y} > n_{\omega x} > n_{2\omega z} > n_{\omega y}$
11	$(n_{\omega x} + n_{\omega z})/2 > n_{2\omega z}$	
00	–	$n_{2\omega z} > n_{\omega x}$

distributions of directions for both types of phase matching, which is presented in Fig. 8. Table 7 presents inequalities for the principal values of refractive indices (similar to those presented in Table 3) for all the projections in Fig. 8. They were obtained from Tables 5 and 6.

In our opinion, the results presented here cover all possible phase-matching distributions for the SHG in biaxial crystals. They show the necessity of revising the results of Ref. [2] for the generation of summation and difference frequencies of laser radiation.

4. Analysis of the configuration diagrams for KTP and RTA crystals

Let us use the results obtained above to analyse changes in projections of two well-known crystals KTP and RTA in their transparency region. The dispersion dependences were taken from Ref. [8] for a KTP crystal and from Ref. [9] for an RTA crystal. The wavelengths of fundamental radiation corresponding to the transitions from one projection to another for a KTP crystal are given in Table 8. One can describe the transitions for this crystal by using the diagram in Fig. 1. The numbers of these transitions are given in the first column of the table.

In the second column, we give the numbers of transitions between the projections in Fig. 6. As the wavelength is increased, the transitions along the set of projections of the KTP crystal from the distribution 00 tend to distribution 22, which is a limiting one, and not to distribution 44, and after that, we have the reverse transition along the same sequence of projections to distribution 00. The wavelength ranges in which phase matching is realised are 741 – 4251 nm for the ssf interaction and 994 – 3106 nm for the sff interaction. At the wavelengths of transitions from one projection to another, which are presented in Table 8, noncritical (with respect to both angles) phase matching (along one of the optic axes of a crystal) is realised.

Table 9 presents the data for the RTA crystal, which are similar to the data in Table 6. Here, only a part of the transitions can be described by using the diagram in Fig. 1. At a wavelength of 1138 nm, the type ssf phase matching along the y axis appears. Subsequently, the transition along the projections 20 – 21 – 22 takes place. As the radiation wavelength is increased further, a decrease in the refractive index $n_x(\omega)$ becomes the dominant factor. As a result, the phase-matching curve intersects the principal crystal planes xy and $xz\,(\theta > \Omega)$, which corresponds to projection 25 in Fig. 6.

Table 8.

Projection		λ/nm	
Fig. 1	Fig. 6	the ssf interaction	the sff interaction
14	00	700	–
14 – 13	00 – 10	741	–
13 – 8	10 – 20	796	–
8 – 7	20 – 21	–	994
7 – 6	21 – 22	–	1079
6 – 7	22 – 21	–	2981
7 – 8	21 – 20	–	3106
8 – 13	20 – 10	4054	–
13 – 14	10 – 00	4251	–
14	00	4500	–

Table 9.

Projection		λ/nm	
Fig. 1	Fig. 6	the ssf interaction	the sff interaction
14	00	700	–
14 – 13	00 – 10	824	–
13 – 8	10 – 20	887	–
8 – 7	20 – 21	–	1138
7 – 6	21 – 22	–	1243
–	22 – 25	–	3285
–	25 – 20	–	3387
8 – 13	20 – 10	4288	–
13 – 14	10 – 00	4627	–
14	00	5800	–

At a wavelength of 3.387356 μm, the condition for the type sff phase-matching along the x axis is fulfilled. This result does not fall into the traditional Hobden classification (see Fig. 1). We do not consider here the reliability of the dispersion dependences of this crystal for the wavelengths above 3 μm. For the RTA crystal at 3.387356 μm (exact phase matching along the x axis), the difference in refractive indices $n_{2\omega x} - 0.5(n_{\omega x} + n_{\omega z})$ corresponding to the appearance of phase matching along the y axis is equal to 0.002. Note that one should not rule out that this wavelength is beyond the limits of applicability of the Sellmeier equations being used. The smallness of this difference suggests the possibility of another transition along the set of projections, in particular, the transition from projection 22 to projection 21, as in the case of the KTP crystal. However, the results obtained above show that projections 25 and 45 in Figs 6 and 8 may occur.

Note that one of the advantages of the use of the diagrams in Figs 6 and 8 is that the sequence of transitions along the set of projections can show the feasibility of the existence of group phase matching, i.e., wavelength-noncritical phase matching which is required for the conversion of ultrashort pulses. For the KTP crystal, the transition observed as the fundamental wavelength increases is of the loop type. This means that wavelength-noncritical phase matching occurs for the distributions corresponding to the 'extreme' state of transitions. For the KTP crystal, this is realised in the 1.96 – 2.012-μm wavelength range for both types of interaction (for different phase-matching angles φ and θ). The spectral width of phase matching is 118 – 135 nm cm$^{1/2}$ for the type ssf interaction and 126 nm cm$^{1/2}$ for the type sff interaction.

Bearing in mind that frequency doublers are used in tunable lasers, the diagrams presented in Figs 6 and 8 make it possible to estimate the angular tuning rate required for this purpose. For example, one can find from Table 6 that the angular rate of tuning of the phase-matching direction for the KTP crystal in the xy plane for the sff interaction is 15.74 pm (angular min)$^{-1}$ in the 994 – 1079 nm wavelength range and 23.15 pm (angular min)$^{-1}$ in the 2981 – 3106 nm range.

5. Noncritical types of phase matching

In conclusion, let us consider one more question, which, in our opinion, was insufficiently discussed in the literature. In most cases, the analysis of stereographic projections does not include the problem of the number of solutions for the phase-matching angles θ that may occur for the given angle φ. This question, as a rule, is also ignored in handbooks on nonlinear crystals. It is obvious that in the case of projections 1 and 2 in Figs 2, 5, and 7, we have the same angle θ corresponding to each angle φ, and the same occurs for projection 5 in Figs 5 and 7. On the other hand, for projections 3 and 4 in Figs 1, 2, and 5 – 8, each angle φ may correspond to two values of angle θ. This possibility is determined by the condition that the derivative of the phase-matching angle with respect to θ vanishes:

$$\frac{\partial\varphi}{\partial\theta} = 0\,, \quad 0 < \theta < \pi\,. \tag{29}$$

Note that, when $\theta = 0$ and $\theta = \pi$ (provided these angles can be achieved for the given wavelength), derivative (29) vanishes because of the symmetry of the phase-matching curve about the principal planes of a crystal.

The fulfilment of condition (29) suggests the presence of phase matching noncritical with respect to the angle, which can be realised not only in the principal planes of a crystal. The choice of a specific phase-matching angle θ is determined by the effective nonlinearity, which depends on the angles φ and θ, and all (angular, spectral, and temperature) phase-matching widths. Note that everything discussed here relates to both ssf and sff phase matching.

Consider the realisation of this regime by using a sodium formate crystal as an example. Fig. 9 presents the phase-matching diagram for the ssf (curve 1) and sff (curve 2) interactions for the fundamental radiation at 532.1 nm. This distribution corresponds to projection 43 in Fig. 6. The phase matching noncritical with respect to the angle is realised at $\varphi = 25.9^\circ$ and $\theta = 43.9^\circ$ (point A) for the ssf interaction and at $\varphi = 53.3^\circ$ and $\theta = 23.7^\circ$ (point B) for the sff interaction.

Figure 10 presents the dependences of the angular phase-matching widths $\Delta\theta$ (a, b) and $\Delta\varphi$ (c, d) for the sff interaction on the fundamental-radiation wavelength λ (a, c) and the angle φ (b, d). All the dependences were calculated along the phase-matching directions for two angles θ (curves 1 and 2). The first angle corresponds to the phase-matching

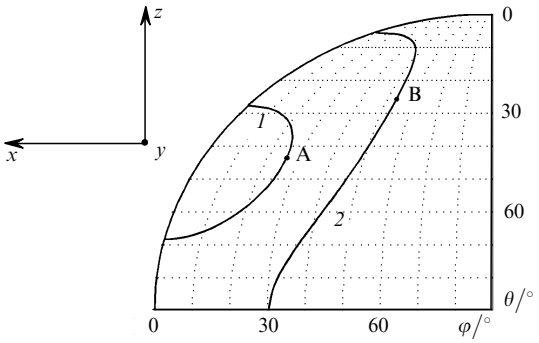

Figure 9. Distribution of phase-matching directions in a SFM crystal.

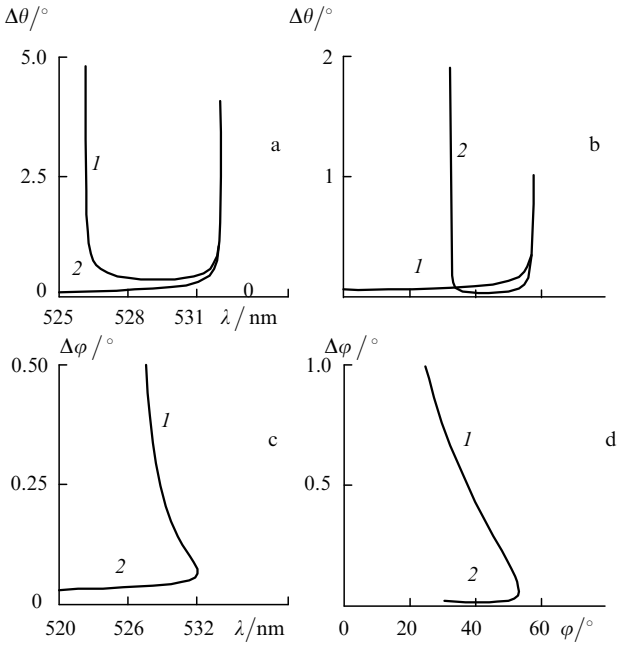

Figure 10. Angular widths of phase matching in a SFM crystal.

curve going upward from the point B in Fig. 9, and the second angle corresponds to the curve going downward. The right-hand maximum of curve 1 in Fig. 10a corresponds to the conversion regime that is noncritical with respect to the angle (point A in Fig. 9), and the left-hand maximum corresponds to the phase-matching in the plane xy that is noncritical with respect to the angle. The latter regime appears in the case where the phase-matching curve for the sff interaction in Fig. 9 gradually approaches the distribution of form 1 in Fig. 5. Similarly, the right-hand maximum in Fig. 10b, where curves 1 and 2 merge together, corresponds to the point B in Fig. 9, and the left-hand maximum to the phase matching in the plane xy that is noncritical with respect to the angle. The dependences of the angular phase-matching widths $\Delta\varphi$ on λ and φ are presented in Figs 10c and 10d. One can see clearly that the phase matching corresponding to the point B in Fig. 9 has a larger angular width.

6. Conclusions

Using the well-known Hobden classification [1], we have provided a complete classification of phase-matching directions for SHG in biaxial crystals with quadratic nonlinearity. The results obtained for the transformation of stereographic projections of biaxial crystals under changes of radiation wavelength demonstrate a strong interrelation between all the projections in the transparent region of a crystal.

The complete diagram of stereographic projections can be advantageously applied to analyse crystals used in practice, for example, to predict noncritical (with respect to the angle, wavelength, and temperature) phase matching. A more detailed comparative analysis of known biaxial crystals based on the results of this paper will be published elsewhere.

The calculation results presented here were obtained by using the LID – SHG (Laser Investigator & Designer – Second Harmonic Generation) code (see http://www.bmstu.ru/~lid).

References

1. Hobden M V J. Appl. Phys. **38** 4365 (1967)
2. Stepanov D Yu, Shigorin V D, Shipulo G P Kvantovaya Elektron. (Moscow) **11** 1957 (1984) [Sov. J. Quantum Electron. 14 1315 (1984)]
3. Handbook of Lasers (Ed. A M Prokhorov), Vol. 2 (Moscow: Sovetskoe Radio, 1978)
4. R L Sutherland Handbook of Nonlinear Optics (New York: Marcel Dekker, 1996)
5. D A Roberts IEEE J. Quantum Electron. **28** 2057 (1992)
6. Yu I Sirotin, M P Shaskol'skaya Foundations of Crystal Physics (Moscow: Nauka, 1979)
7. V G Dmitriev, G G Gurzadyan, D N Nikogosyan Handbook of Nonlinear Optical Crystals (Berlin: Springer, 1996)
8. Fan T Y, Huang C F, Hu B Q, et al. Appl. Opt. **26** 2390 (1987)
9. L K Cheng, L T Cheng, et al. J Crystal Growth **137** 107 (1994)